Stability Parameter and Roll Rate from Early Re-Entry Radar or Optical Data

R. L. Henry*
U.S. Air Force Systems Command, Wright-Patterson Air Force Base, Ohio

The modulation of the early re-entry intensity of optical emissions and radar range by the angular motion of a rolling re-entry vehicle is examined. The theoretical spectra of the modulation in the frequency space canonical to the square root of the air density at the vehicle altitude are generated. Transforms of length sufficient to resolve roll-related features without masking by the variation of the pitch oscillation frequency with vehicle altitude are possible in this frequency domain. It is shown that modulation mechanisms that depend linearly and quadratically on vehicle angle of attack result in up to six frequency components in this space. This transform technique provides a means to determine altitude-dependent stability parameter and roll-rate altitude profiles from optical or radar re-entry data.

Nomenclature

A = aerodynamic reference area for moment coefficients
$B_1 e^{i\psi_1}$, $B_2 e^{i\psi_2}$ = alternative expressions for initial conditions
C_{l0}, C_{lp} = aerodynamic roll-driving and damping-moment coefficients, respectively
$C_{m\alpha}$ = aerodynamic pitching-moment coefficient derivative
$C_1' e^{i\phi_1}$, $C_1' e^{i\phi_2}$ = exponential function coefficients in angular solution
C_1'', C_2'' = Bessel function coefficients set by initial conditions
D, D_α, D_β = complex, real, and imaginary parts of coefficients of linear terms in expansion of radar or optical signal at sensor
E, E_α, E_β = complex, real and imaginary parts of coefficients of quadratic terms in expansion of radar or optical signal at sensor
H = reference altitude parameter in exponential expression for air density
I, I_x = pitch and roll moments of inertia
i = $(-1)^{1/2}$
$J(t)$ = radar or optical signal at sensor
$J_b(t)$ = slowly varying bias in $J(t)$
$J_\nu(\theta)$, $Y_\nu(\theta)$ = Bessel functions of first and second kind of order ν
$J_0(t)$ = zero-order term in expansion of $J(t)$
l = aerodynamic reference length for moment coefficients
P, Q = coefficients of circular functions in Hankel's asymptotic expansion for Bessel's functions
P_s = stability parameter
p = roll rate
p_0 = initial roll rate at initial time t_0
R = ratio of quadratic to linear contributions to angular expansion of radar or optical data
S = normalized modulation of radar or optical data
s = roll-related frequency canonical to $\sqrt{\rho}$
$T(\omega)$ = Fourier spectrum of radar or optical data at frequency ω canonical to $\sqrt{\rho}$
t = time
v = vehicle velocity
w = roll-related damping function
X = $\theta - \frac{1}{2}\nu\pi - \frac{1}{4}\pi$
α, β = pitch and yaw angles
γ = re-entry angle
θ = pitch-related frequency canonical to $\sqrt{\rho}$
$(\nu)_k$ = Pochhammer's symbol
Ξ = solution to Eq. (15)
ξ = complex angle of attack
ρ = air density
ρ_n = parameter in exponential expression for air density
ρ_1, ρ_2 = air density values at limits of Fourier transform
ϕ_3 = phase of D
ϕ_4 = phase of E
ω = modulation frequency canonical to $\sqrt{\rho}$
$(\dot{})$ = time derivative

I. Introduction

BOTH the stability parameter and the roll rate of a re-entry vehicle (RV) as functions of altitude during the early portion of re-entry are of interest to those attempting to understand the characteristics of a missile system. Reference 1 describes techniques used by many analysts for the extraction of this information from optical data collected during the re-entry of RV's whose roll rate either differed greatly from the natural pitch oscillation frequency or was exactly the same because the RV was locked into lunar motion due to roll resonance. This paper examines the body-motion-induced modulation in radar and optical re-entry data by nonlifting, axially symmetric RV's. In particular, the expected spectra in the frequency domain canonical to the square root of the air density at the RV altitude is examined. In this domain, transforms of lengths sufficient to resolve roll-related features can be performed without masking due to changes in the planar oscillation frequency. Body-motion-induced modulation by these vehicles can result in a rich spectrum in this domain with up to six frequency components. The extension to include other ef-

Received Nov. 19, 1987; revision received April 27, 1988.

*Aerospace Engineer, Foreign Technology Division. Senior Member AIAA.

fects such as lift is straightforward, but beyond the intended scope of this effort.

RV characteristics can be obtained by comparing field and theoretical spectra. This technique is more general in that it can utilize a motion solution which is applicable in the high-altitude region where the roll and natural pitch frequencies are approximately, but not necessarily exactly, equal as well as when they differ greatly. The novel features of this approach are the independent variable used in the frequency analysis of the field data and the incorporation of a complete angular motion solution, including the effects of RV roll, into the theoretical signature-modulation model. The description is organized as follows: The modulation mechanism for both the optical and the radar case is described, the angular motion solution is presented, and several examples illustrating features of the frequency content of the theoretical modulation implied by the resulting angular solution are shown.

II. Modulation Mechanism

Consider the modulation imparted by this motion to the optical emissions from the surface of an RV. Initially assume that the optical sensor views the RV along its velocity vector as shown in position P of Fig. 1. The heating rate of the RV heat shield by the wind stream increases as the angle between the incident air and the normal to the heat shield surface decreases. A larger area receives the nearly normal aerodynamic heating when the RV is in positions A and C of Fig. 1 than when it is aligned with the airflow as in position B. The surface temperature of the RV heat shield and hence its optical emissions increase with heating rate (in the absence of phase-transition phenomena). Two optical flashes per mechanical cycle are observed because the sensor receives more radiation when the RV is in positions A and C than when it is in position B.

Now consider the case where the sensor is displaced along a direction parallel to the oscillation plane such that its line of sight is not parallel to the RV's velocity vector as illustrated in position P′of Fig. 1. When the RV is in position B, less radiation is observed than when it is in position C, but more than when it is in position A because the radiation from the windward heated surface in position A is partially shadowed from the sensor by the RV itself. Hence, this viewing angle results in one optical cycle per mechanical cycle. In general, the optical modulation due to RV surface emission is a combination of the above cases whose relative mixtures are determined by the viewing conditions. Since the angle between the sensor line of sight and the normal to the plan of oscillation of the RV has a large effect on the resulting modulation and since this plane rotates as the RV rolls, the overall signal is also modulated by RV roll.

The RV motion also modulates the optical emissions from ablation products in the RV wake. The intensity of these emissions is directly related to the quantity of these products which depends on both the heated area of the heat shield and its material properties, the heating rate, and the time necessary for the emitting species to cool sufficiently for their emissions to become negligible. The wake emissions are dependent on the vehicle orientation because the high heating rate area of the RV is increased when the RV symmetry axis is misaligned with its velocity vector. This modulation is almost independent of the viewing angle (and therefore RV roll) because RV's are too small to shadow a significant portion of the wake for most viewing geometries and optical bandpasses (effective wake dimensions are dependent on optical bandpass). This mechanism results in two optical flashes per mechanical cycle. The total optical modulation is due to the combination of the modulation of the RV surface emissions and wake emissions.

The radar-range data is also modulated by the body motion. Although some work has been performed to extract the stability parameter from radar data collected at low altitudes, none has been applied to the early re-entry region. Consider the case where the radar views the RV from position P of Fig. 1. After subtracting the average decrease of the range to the RV's center of mass, the residual range to a scatterer at the RV nose is larger when the RV is in positions A and C in this figure than when it is position B. This results in two modulation events per mechanical cycle. When the radar is moved in a direction perpendicular to the RV velocity vector and parallel to the RV oscillation plane as shown in position P′of Fig. 1, the residual range to RV nose increases as its orientation progresses from position A through B to C. For this case, there is one modulation event per mechanical cycle. For both cases, the frequency of the range residuals to other scattering centers varies at the same frequency but with different amplitudes and phases. In general, the modulation of the radar-range residuals is a combination of the two cases discusses above whose relative weights depends upon the viewing geometry. The radar-range residuals are modulated by the rotation of the oscillation plane of a rolling RV because this rotation changes the angle between the viewing direction and the oscillation plane.

The change in the planar oscillation frequency with RV altitude complicates the measurement of the various frequencies present in the data. Fourier transforming a segment of the signal yields a spectrum whose resolution is inversely proportional to the length of the segment. If time is used as the independent variable in this transform, the changes in the planar oscillation frequency with RV altitude will completely mask any roll-related features in any data segment of sufficient length to otherwise resolve these features. This masking can be avoided if the independent variable is changed to one that varies with altitude, such that its variation approximately compensates for the change in planar oscillation frequency. The square root of the air density at the RV altitude is a suitable independent variable.

Both the optical and the radar data include a large bias that varies relatively slowly with altitude. In the optical case, this bias is due to the increase in the overall emissions caused by the increase in surface emissions due to the increase in surface temperatures and the increase in wake emissions due to the increased ablation rates induced by the increased aerodynamic heating as the RV altitude decreases. In the radar case, this bias is due to the decrease in the range as the RV center of mass moves toward the radar. Both types of data also have amplitude envelopes which vary with altitude due to the change in viewing conditions, the RV geometry, and the damping of the magnitude of the RV's angle of attack as the air density increases. The envelope of the optical modulation also varies due to the properties of the heat-shield material and the altitude-dependent heating rates. Regardless of their origin, these features must be removed from the data before transformation to avoid masking the desired features by the finite width of the

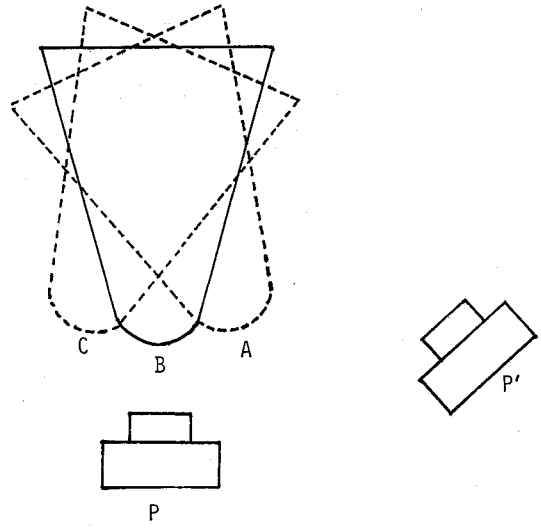

Fig. 1. RV orientations A, B, and C and sensor positions P and P′ considered in text.

large low-frequency components induced by the bias and envelope functions.

To predict the modulation spectra for a given RV, it is necessary to describe the above phenomena in a quantitative manner. For small pitch and yaw angles, the signal to be transformed may be expressed as a power series in these angles. The coefficients of this expansion are slowly varying functions of altitude determined by viewing conditions, material properties, and similar quantities. The zeroth-order term corresponds to the slowly varying bias mentioned above, the linear terms correspond to the modulation mechanisms, which result in a single modulation event per mechanical cycle, and the quadratic terms correspond to the mechanisms, which result in two modulation events per mechanical cycle. For an axially symmetric RV, it is possible to choose the coordinate system to eliminate terms containing the product of the pitch and yaw angles. In this system, the signal $J(t)$ observed by the sensor can be expressed as

$$J(t) = J_0(t) + D_\alpha(t)\alpha(t) + D_\beta(t)\beta(t) + E_\alpha(t)\alpha^2(t) + E_\beta(t)\beta^2(t) \tag{1}$$

where $J_0(t)$ is the signal seen by the sensor when the RV is in the aligned orientation and the quantities $D_\alpha(t)$, $D_\beta(t)$, $E_\alpha(t)$, and $E_\beta(t)$ are the expansion coefficients of the terms in which they appear.

III. Angular Motion Solution

Many treatments of the theoretical angular motion of an RV are found in the literature. References 2–15 provide a representative, but by no means exhaustive, set of examples of the early work in this area. A much more extensive bibliography is included in the excellent review article by Platus.[16] References 2–6 are particularly applicable since they account for the effects on the RV motion of the variation in the air density with RV altitude. Other effects such as lift (Ref. 5) and ablation (Ref. 13) have also been considered. The motion solution considered here is applicable to an axially symmetric, nonlifting RV when ablation effects are negligible and the maximum aerodynamic is sufficiently small that only the linear aerodynamic terms are significant. Extending this solution to include other effects is straightforward.

In the high endoatmospheric portion of the RV trajectory, the center of mass and the angular motions may be separated because of the negligible drag changes induced by small angles of attack and the RV's almost constant velocity vector. In the aeroballistic coordinate system, the angular equations of motion are

$$I_x\dot{p} - \tfrac{1}{2}\rho v^2 C_{l0} Al - \tfrac{1}{2}\rho v^2 \frac{C_{lp} Al^2 p}{v} = 0 \tag{2}$$

$$I\ddot{\alpha} - \dot{\beta} p I_x - \tfrac{1}{2}\rho v^2 C_{m\alpha} Al\,\alpha = 0 \tag{3}$$

$$I\ddot{\beta} + \dot{\alpha} p I_x - \tfrac{1}{2}\rho v^2 C_{m\alpha} Al\,\beta = 0 \tag{4}$$

The roll moment is assumed to vary linearly with roll rate. For a truly axially symmetric RV, the quantity C_{l0} must vanish because an axially symmetric RV cannot have a preferred roll direction. The above equations are also applicable to an almost axially symmetric RV obtained by adding spin fins, a spiral tape-wrapped heat shield, or similar modifications to a truly axially symmetric RV if its moment of inertia tensor is diagonal, one of the eigenvectors of the moment of inertia tensor of the modified RV coincides with the axis of symmetry of the unmodified RV, and if the moments of inertia corresponding to the other eigenvectors are identical to each other.

The stability parameter is customarily defined in terms of the pitching moment coefficient derivative as

$$P_s = -C_{m\alpha} Al/I \tag{5}$$

Equations (2–4) constitute a set of three coupled equations for the pitch and yaw angles, α and β, and the roll rate p. Since only the derivative of the roll rate only appears in Eq. (2), the roll rate can be obtained by numerical integration using values of C_{l0} and C_{lp} that have have been averaged over the instantaneous cyclical variations in α and β.

$$p(t) = \exp\left\{\int_{t_0}^{t} \frac{1}{2}\rho v^2 \frac{C_{lp} Al^2}{I_x v}\,dt'\right\}\left\{\int_{t_0}^{t} \frac{1}{2}\rho v^2 \frac{C_{i0} Al}{I_x} \times \exp\left(-\int_{t_0}^{t''} \frac{1}{2}\rho v^2 \frac{C_{lp} Al^2}{I_x v}\,dt'\right)dt'' + p_0\right\} \tag{6}$$

where t' and t'' are integration variables. Equations (3) and (4) can be combined into a single equation by defining a complex angle of attack ξ

$$\xi = i\alpha + \beta \tag{7}$$

Substituting this into Eqs. (3) and (4) yields

$$\ddot{\xi} - ip(I_x/I)\dot{\xi} - \frac{C_{m\alpha} Al\,\tfrac{1}{2}\rho v^2 \xi}{I} = 0 \tag{8}$$

To show the variation of air density with altitude and hence time, it is helpful to write it as

$$\rho = \rho_n \exp\{(vt\,\sin\gamma)/H\} \tag{9}$$

where H and ρ_n are atmospheric functions that vary slowly with RV altitude. Combining Eqs. (8) and (9) yields

$$\ddot{\xi} - ip(I_x/I)\dot{\xi} - \frac{C_{m\alpha} Al}{I}\tfrac{1}{2}\rho_n v^2 \exp\{(vt\,\sin\gamma)/H\}\xi = 0 \tag{10}$$

The altitude variations of the slowly varying functions $C_{m\alpha}$, p, v, γ, ρ_n, and H will be handled by solving Eq. (10) for ξ as an explicit function of these quantities and the independent variable and then generating values for ξ numerically using the known altitude profiles of these quantities. Define the new independent variable θ by

$$\theta = \left(\frac{2H^2 P_s}{\sin^2\gamma}\right)^{1/2}\sqrt{\rho} \tag{11}$$

$$\theta = \left(\frac{2H^2 \rho_n P_s}{\sin^2\gamma}\right)^{1/2}\exp\{vt\,\sin\gamma/(2H)\} \tag{12}$$

If this is substituted into Eq. (10) and if the derivatives of the quantities $C_{m\alpha}$, v, γ, ρ_n, H, and p are negligibly small, Eq. (10) becomes

$$\frac{\partial^2\xi}{\partial\theta^2} + \frac{1}{\theta}\frac{\partial\xi}{\partial\theta} + \xi = \frac{2ipH\,(I_x/I)}{v\,\sin\gamma}\frac{1}{\theta}\frac{\partial\xi}{\partial\theta} \tag{13}$$

Now take ξ to be of the form

$$\xi = \theta^{ip(I_x/I)H/(v\,\sin\gamma)}\Xi \tag{14}$$

then

$$\theta^2\frac{\partial^2\Xi}{\partial^2\theta} + \theta\frac{\partial\Xi}{\partial\theta} + \Xi\left[\theta^2 - \left(\frac{ip(I_x/I)H}{v\,\sin\gamma}\right)^2\right] = 0 \tag{15}$$

which is Bessel's equation of order ν, where

$$\nu = \frac{ip(I_x/I)H}{v\,\sin\gamma} \tag{16}$$

This has the solution

$$\Xi = C_1'' J_\nu(\theta) + C_2'' Y_\nu(\theta) \tag{17}$$

where the coefficients of the Bessel's functions, C_1'' and C_2'', are determined by the initial conditions. Combining Eqs. (11), (14), and (17),

$$\xi = \exp\left\{ip(I_x/I)\frac{H}{v\sin\gamma}\ell n\left[\left(\frac{2H^2P_s}{\sin^2\gamma}\right)^{1/2}\sqrt{\rho}\right]\right\} \times\left\{C_1''J_\nu\left[\left(\frac{2H^2P_s}{\sin^2\gamma}\right)^{1/2}\sqrt{\rho}\right]+C_2''Y_\nu\left[\left(\frac{2H^2P_s}{\sin^2\gamma}\right)^{1/2}\sqrt{\rho}\right]\right\} \tag{18}$$

Equations (6), (16), and (18) constitute the desired angular solution. To properly understand the modulation implied by this solution, it is helpful to express the Bessel functions using Hankel's asymptotic expansion:

$$J_\nu(\theta) = \left(\frac{2}{\pi\theta}\right)^{1/2}\{P(\nu,\theta)\cos X - Q(\nu,\theta)\sin X\} \tag{19}$$

$$Y_\nu(\theta) = \left(\frac{2}{\pi\theta}\right)^{1/2}\{P(\nu,\theta)\sin X + Q(\nu,\theta)\cos X\} \tag{20}$$

where

$$x = \theta - \tfrac{1}{2}\nu\pi - \tfrac{1}{4}\pi \tag{21}$$

$$P(\nu,\theta) = \sum_{k=0}^{\infty}(-1)^k\frac{(\nu,2k)}{(2\theta)^{2k}} \tag{22}$$

$$Q(\nu,\theta) = \sum_{k=0}^{\infty}(-1)^k\frac{(\nu,2k+1)}{(2\theta)^{2k+1}} \tag{23}$$

Hankel's symbol (ν,k) can be expressed in terms of Pochhammer's symbol $(\nu)_k$ by

$$(\nu,k) = \frac{(-1)^k}{k!}(\tfrac{1}{2}-\nu)_k(\tfrac{1}{2}+\nu)_k \tag{24}$$

For typical values encountered in intercontinental ballistic missile RV re-entries, the series in Eqs. (22) and (23) converge very rapidly. For many cases (except at high altitudes or roll rates), P and Q are very close to unity and zero, respectively. Combining Eqs. (18), (19), and (20) and simplifying the notation by introducing the symbols

$$s = \left\{\frac{p(I_x/I)H}{\sqrt{\rho}\,v\sin\gamma}\ell n\left[\left(\frac{2H^2P_s}{\sin^2\gamma}\right)^{1/2}\sqrt{\rho}\right)\right\}\sqrt{\rho} \tag{25}$$

$$w = \frac{\pi p(I_x/I)\mathrm{H}}{2v\sin\gamma} \tag{26}$$

$$B_1e^{i\psi_1} = (C_1'' - iC_2'') \tag{27}$$

$$B_2e^{i\psi_2} = (C_1'' + iC_2'') \tag{28}$$

$$C_1'e^{i\phi_1} = B_1e^{i\psi_1}\{P + iQ\}e^{-i\pi/4} \tag{29}$$

$$C_2'e^{i\phi_2} = B_2e^{i\psi_2}\{P - iQ\}e^{i\pi/4} \tag{30}$$

the angular solution reduces to the simple result

$$\xi = \frac{1}{(2\pi\theta)^{1/2}}\{e^wC_1'\exp[i(\theta+s+\phi_1)] + e^{-w}C_2'\exp[-i(\theta-s-\phi_2)]\} \tag{31}$$

In this expression, θ and s are the products of the independent variable $\sqrt{\rho}$ and the planar and the roll-related frequencies [the bracketed coefficients of $\sqrt{\rho}$ in Eqs. (11) and (25)], respectively which are canonical to $\sqrt{\rho}$. The roll-related frequency is dependent upon $\sqrt{\rho}$ but varies slowly with altitude at high altitudes. The quantity w is an exponential decay or growth factor proportional to roll rate. The quantities B_1 and B_2 are the moduli and ψ_1 and ψ_2 are the phases of alternative expressions for the complex numbers representing the initial conditions of the complex angle of attack. The quantities C_1' and C_2' are functions of the initial conditions which vary slowly with altitude and roll rate due to their dependence on the Hankel symbols. Equation (31) illustrates that the complex angle of attack can be expressed as the sum of terms which oscillate at the sum and the difference of the planar and the roll-related frequencies canonical to $\sqrt{\rho}$. The relative importance of the two terms depends on the initial conditions and the roll rate. For fixed values of the initial conditions, the ratio of the contributions of the sum term to the difference term increases approximately exponentially with increasing roll rate.

IV. Modulation Implied by Motion Solution

Since examination of the actual signal is not particularly illuminating, the details of the motion are best revealed in the magnitude of the Fourier transform of the signal defined by

$$T(\omega) = \int_{\sqrt{\rho_1}}^{\sqrt{\rho_2}} Se^{-i\sqrt{\rho}\omega}\,\mathrm{d}(\sqrt{\rho}) \tag{32}$$

where $S(\sqrt{\rho})$ is the signal at $\sqrt{\rho}$ after the dependence on the bias and the envelope functions have been removed, and $\sqrt{\rho_1}$ and $\sqrt{\rho_2}$ are the integration endpoints in root air-density space. To understand this modulation spectra, it is helpful to consider three cases: A, when $E\alpha$ and E_β in Eq. (1) both vanish; B, when D_α and D_β in Eq. (1) both vanish; and C, when neither set vanishes.

To illustrate the features of the various cases, theoretical modulation spectra of an RV with an altitude-independent stability parameter of 0.004 m/kg and a constant roll rate of 165 deg/s were generated. The RV was assumed to be following a trajectory for an RV with velocity of 6.28 km/s and a re-entry angle of 24 deg at an altitutde of 120 km, a hypersonic ballistic coefficient of 7000 kg/m^2 and a ballistic coefficient Mach-number variation which follows a Berman profile for a 7.5 deg, 0.26 bluntness ratio sphere cone (see Ref. 17). The altitude variation of air density was taken to be that of the 1962 U. S. Standard Atmosphere.[18] For this case, the RV moment of inertia ratio was set a 0.1 and the initial conditions were taken to yield $\psi_1 = 135$ deg, $\psi_2 = -90$ deg, and $B_1/B_2 = 0.1$. The points input to the Fourier transforms were evenly spaced in time and hence unevenly spaced in $\sqrt{\rho}$ space. The bandwidths of the resulting spectra were assumed to be determined by the widest spacing of input points in $\sqrt{\rho}$ space. All of the spectra were normalized such that their largest values were equal to unity.

A. Linear Case

When E_α and E_β vanish, Eq. (1) can be expressed elegantly by defining a complex function

$$D = |D|e^{i\phi}3 \tag{33}$$

$$D = D_\beta + iD_\alpha \tag{34}$$

Inserting this into Eq. (1),

$$J(t) = J_0(t) + Re(D^*\xi) \tag{35}$$

The envelope of the oscillations represented by the terms in Eq. (35) each have different dependence on roll rate. For definiteness, the envelope function will be taken to be the coefficient of the cosine term which depends on the difference of θ and s.

$$\langle J(t) - J_0(t)\rangle = \frac{e^{-w}C_2'}{(2\pi\theta)^{1/2}}|D| \tag{36}$$

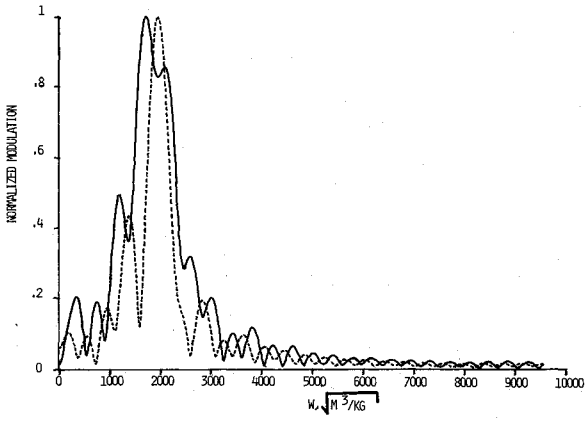

Fig. 2 Modulation spectra of rolling (solid line) and a nonrolling (dashed line) vehicles for linear case in 81.88–58.03 km altitude region.

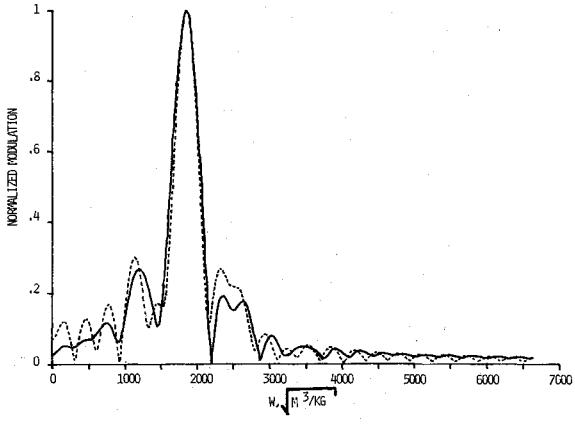

Fig. 3 Modulation spectra of rolling (solid line) and a nonrolling (dashed line) vehicles for linear case in 71.89–52.05 km altitude region.

With these definitions, the normalized signal S, becomes

$$S = \frac{J(t) - J_0(t)}{\langle J(t) - J_0(t) \rangle} \tag{37}$$

$$S = e^{2w}(C_1'/C_2') \cos(\theta + s + \phi_1 - \phi_3) + \cos(\theta - s - \phi_2 + \phi_3) \tag{38}$$

This modulation spectrum consists of a doublet with a spacing equal to twice the roll-related frequency. The relative intensity of the sum term increases exponentially at the expense of that of the difference term with increasing roll rate. The effects of high roll rates are manifest as a shift in the center frequency of the single visible component. The change in the roll-related frequency with altitude strongly influences the Fourier spectra of Eq. (38).

Consider a transform over a change of $\sqrt{\rho}$ sufficient to yield a resolution comparable to the doublet splitting. Transforming between 81.88 and 58.03 km with viewing conditions such that $\phi_3 = 45$ deg, a sampling rate of 59.78 frames/s [equivalent to bandwidth of 9568.1 $(m^2/kg)^{1/2}$], and a suitable choice of initial conditions, the doublet structure is clearly visible in the solid line in Fig. 2. The spectra for an otherwise identical nonrolling RV observed under the same conditions is shown by the dashed line in Fig. 2. The single peak of this latter spectrum falls between the two major features of the former spectrum.

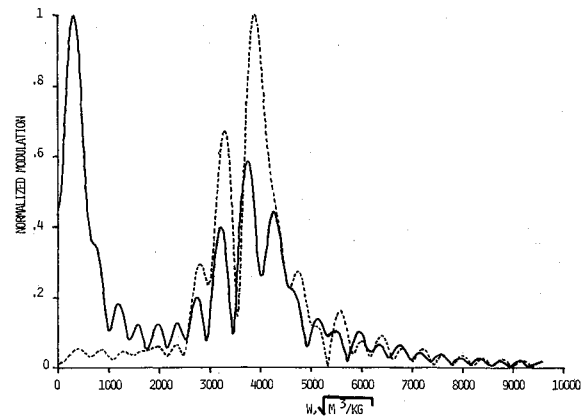

Fig. 4. Modulation spectra of rolling (solid line) and a nonrolling (dashed line) vehicles for quadratic case in 81.88–58.03 km altitude region.

At somewhat lower altitudes, the change in the roll-related frequency with altitude is sufficient to wash out this doublet structure. The altitude dependence of air density prevents simultaneously fixing the resolution and bandwidth of the transform, the ratio of the resolution to the roll-related frequency, and the effective framing rate of the signal because the signal points are equally spaced in time rather than in $\sqrt{\rho}$ space. With the same roll rate, trajectory, viewing conditions, effective framing rate considered earlier, and ratio of the transform resolution to the roll-related frequency considered earlier, the spectra of rolling and nonrolling RV's between 71.89 and 52.05 km are shown by the solid and dashed lines, respectively, in Fig. 3. Notice that the bandwidth of these spectra is only 6640.7 $(m^2/kg)^{1/2}$.

B. Quadratic Case

When D_α and D_β vanish, it is helpful to write the remaining viewing coefficients as

$$E_\alpha = |E| \cos\phi_4 \tag{39}$$

$$E_\beta = |E| \sin\phi_4 \tag{40}$$

As in the linear case, each of the various terms obtained by combining Eqs. (1), (31), (39), and (40) have different coefficients. Take the envelope function to be the coefficient of the cosine term involving twice the difference of θ and s.

$$\langle J(t) - J_b(t) \rangle = |E| \frac{e^{-2w}C_2'^2}{4\pi\theta} \tag{41}$$

The presence or absence of RV roll also effects the nonoscillatory bias J_b, which includes other terms besides the J_0 term. After these are subtracted, the normalized signal for the rolling subcase becomes

$$S = \frac{J(t) - J_0(t) - |E| \frac{e^{-2w}C_2'^2}{4\pi\theta} (\cos\phi_4 + \sin\phi_4)[1 + e^{4w}(C_1'/C_2')^2]}{|E| \frac{e^{-2w}C_2'^2}{4\pi\theta}} \tag{42}$$

$$= (\cos\phi_4 - \sin\phi_4) \cos[2(\theta - s) - 2\phi_2] + e^{4w}(C_1'/C_2')^2(\cos\phi_4 - \sin\phi_4) \cos[2(\theta + s) + 2\phi_1] + 2e^{2w}(C_1'/C_2')\{\cos\phi_4 \cos[2\theta - (\phi_1 + \phi_2)] + \sin\phi_4 \cos[2\theta + (\phi_1 - \phi_2)] + \cos\phi_4 \cos[2s - (\phi_1 - \phi_2)] - \sin\phi_4 \cos[2s + (\phi_1 + \phi_2)]\} \tag{43}$$

For the nonrolling subcase, the signal becomes

$$S = \left\{ |E| \frac{e^{-2wC_2'^2}}{4\pi\theta} \right\}^{-1} [J(t) - J_0(t) - |E| \frac{e^{-2wC_2'^2}}{4\pi\theta} \times [1 + e^{4w}(C_1'/C_2')^2](\cos\phi_4 + \sin\phi_4) + 2e^{2w}(C_1'/C_2')$$
$$\times \{\cos\phi_4 \cos(\phi_1 - \phi_2) - \sin\phi_4 \cos(\phi_1 + \phi_2)\} = (\cos\phi_4 - \sin\phi_4)\{e^{4w}(C_1'/C_2')^2 \cos(2\theta + 2\phi_1) + \cos(2\theta - 2\phi_2)\}$$
$$+ 2e^{2w}(C_1'/C_2') \times \{\cos\phi_4 \cos[2\theta - (\phi_1 + \phi_2)] + \sin\phi_4 \cos[2\theta + (\phi_1 - \phi_2)]\} \quad (44)$$

For the second-order case, the modulation spectrum consists of a triplet with features at twice the planar frequency, twice the sum of the planar and the roll-related frequencies, and twice the difference of the planar and the roll-related frequencies and a singlet at twice the roll-related frequency. With increasing roll rate, the intensities of the sum term increases exponentially at the expense of that of both the double the planar frequency term and the double the roll-related frequency term. These terms, in turn, increase exponentially at the expense of that of the difference term. At high roll rates, the effects of RV roll are evident in the presence of the roll-related singlet feature and in the distortion of the side lobe structure of the spectrum.

The change in the roll-related frequency with altitude also has a strong influence on the Fourier spectra of Eq. (43). Under the same conditions and transform limits as those used to generate Fig. 2 and with $\phi_4 = 0$, the triplet and singlet structures are clearly visible as shown by the solid line in Fig. 4. The spectrum for an otherwise identical nonrolling RV observed under these same conditions is shown by the dashed line in the same figure. Notice the spurious feature due to the side lobe adjacent to the central peak. At somewhat lower altitudes, the change in the roll-related frequency is sufficient to wash out the triplet structure. This effect is illustrated by the solid line in Fig. 5 for a rolling RV with the same viewing conditions as those used to generate Fig. 4 and the same transform limits as those used to generate Fig. 3. Although the triplet structure is obscured by the side lobes, the singlet at twice the roll-related frequency is still clearly visible. The spectrum for a nonrolling RV under the same viewing conditions and transform limits is shown by the dashed line in Fig. 5. The absence of the effects of RV roll are best observed despite the enchanced side lobe structure by noting the absence of the roll-related singlet.

C. Combined Case

When neither sets of coefficients vanish, the various cosine terms have a different dependence on RV roll rate. Since the linear and quadratic terms depend differently on $\sqrt{\rho}$, their relative importance changes with altitude. Take the envelope function to be the same as that in the first-order case. It is convenient to define the ratio

$$R = |E|/|D| \quad (45)$$

As in the second-order case, the presence or absence of RV roll effects the nonoscillatory bias. After this is subtracted, the normalized signal for the rolling subcase becomes

$$S = \frac{J(t) - J_0(t) - |E| \frac{e^{-2wC_2'^2}}{4\pi\theta} (\cos\phi_4 + \sin\phi_4)[1 + e^{4w}(C_1'/C_2')^2]}{\frac{e^{-wC_2'}}{(2\pi\theta)^{1/2}} |D|} \quad (46)$$

$$= \cos(\theta - s - \phi_2 + \phi_3) + e^{2w}(C_1'/C_2') \cos(\theta + s + \phi_1 - \phi_3) + \frac{e^{-wC_2'R}}{2(2\pi\theta)^{1/2}} [e^{4w}(C_1'/C_2')^2(\cos\phi_4 - \sin\phi_4)\cos[2(\theta + s) + 2\phi_1]$$
$$+ (\cos\phi_4 - \sin\phi_4) \cos[2(\theta - s) - 2\phi_2] + 2e^{2w}(C_1'/C_2')\{\cos\phi_4 \cos[2\theta - (\phi_1 + \phi_2)] + \sin\phi_4 \cos[2\theta + (\phi_1 - \phi_2)]$$
$$+ \cos\phi_4 \cos[2s - (\phi_1 - \phi_2)] - \sin\phi_4 \cos[2s + (\phi_1 + \phi_2)]\}] \quad (47)$$

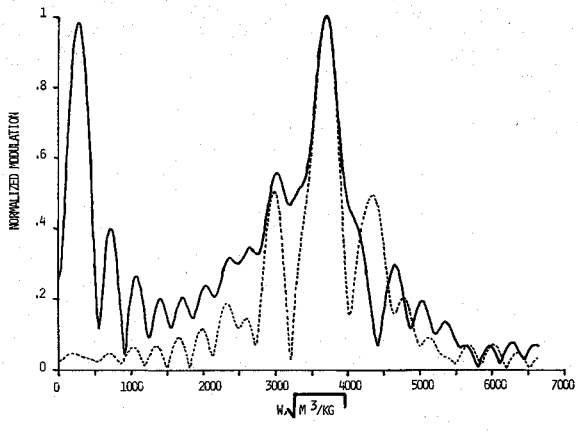

Fig. 5 Modulation spectra of rolling (solid line) and nonrolling (dashed line) vehicles for quadratic case in 71.89–52.05 km altitude region.

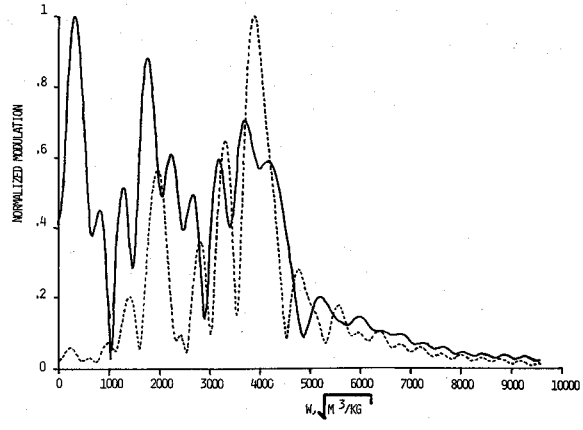

Fig. 6 Modulation spectra of rolling (solid line) and a nonrolling (dashed line) vehicles for combined case in 81.88–58.03 km altitude region.

For the nonrolling subcase, the signal becomes

$$S = \left(|D| \frac{e^{-wC_2'^2}}{(2\pi\theta)^{1/2}} \right)^{-1} \left(J(t) - J_0(t) - |E| \frac{e^{-2wC_2'^2}}{(4\pi\theta)} [1 + e^{+4w(C_1'/C_2')^2}](\cos\phi_4 + \sin\phi_4) \right.$$
$$\left. + 2e^{2w(C_1'/C_2')}\{\cos\phi_4 \cos(\phi_1 - \phi_2) - \sin\phi_4 \cos(\phi_1 + \phi_2)\} \right) = \cos(\theta - \phi_2 + \phi_3) + e^{2w(C_1'/C_2')^2} \cos(\theta + \phi_1 - \phi_3)$$
$$+ \frac{e^{-wC_2'R}}{2(2\pi\theta)^{1/2}} \left((\cos\phi_4 - \sin\phi_4)\{e^{4w(C_1'/C_2')^2} \cos(2\theta + 2\phi_1) + \cos(2\theta - 2\phi_2)\} + 2e^{2w(C_1'/C_2')}\{\cos\phi_4 \cos[2\theta - (\phi_1 + \phi_2)] \right.$$
$$\left. + \sin\phi_4 \cos[2\theta + (\phi_1 - \phi_2)]\} \right) \tag{48}$$

This modulation spectrum consists of a doublet with features at the sum and the difference of the planar and the roll-related frequencies, a triplet with features at twice the planar frequency, twice the sum of the planar and the roll-related frequencies, and twice the difference of the planar and the roll-related frequencies, and a singlet at twice the roll-related frequency. The relative intensities of the terms in Eqs. (47) and (48) which result from the linear terms in Eq. (1) increase at the expense of those from the quadratic terms as the fourth root of air density and exponentially with increasing roll rate. The relative intensities of the various components of the linearly derived terms and the various components of the quadratically derived terms are the same as those described in their respective sections.

The altitude variation of the roll-related frequency also has a strong influence on the Fourier spectra of Eq. (48). Under the same conditions and transform limits as those used to generate Figs. 3 and 5 and with $B_2R = 550$, the various features are clearly visible as shown by the solid line in Fig. 6. The theoretical modulation expected from an otherwise identical nonrolling RV observed under these same conditions is shown by the dashed line in Fig. 6. The spurious feature due to the side lobe adjacent to the second-order peak which was present in the quadratic case is also visible in this figure.

At somewhat lower altitudes, the change in the roll-related frequency is again sufficient to wash out the doublet and the triplet structures. As in the second-order case, the effects of RV roll are evident in the presence of the weak roll-related singlet feature and in the distortion of the side lobe structure of the spectrum. This effect is illustrated for rolling and nonrolling RV's by the solid and dashed lines, respectively, in Fig. 7 under the same conditions and transform limits as those used to generate Figs. 3 and 5. The reduction in the intensities of the quadratic features relative to those of the linear features compared to their relative strengths in the higher altitude figures is due to the fourth root of air density dependence in Eq. (47) and (48).

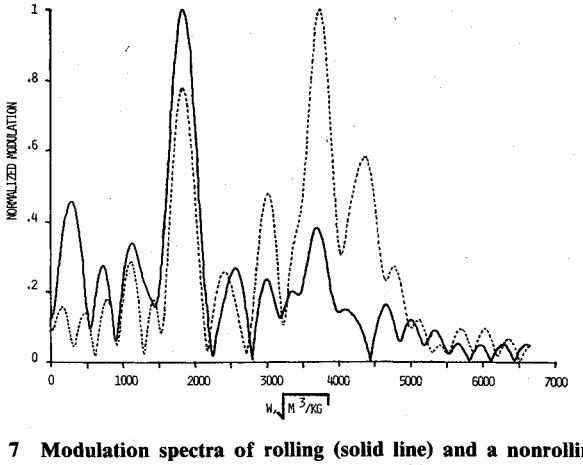

Fig. 7 Modulation spectra of rolling (solid line) and a nonrolling (dashed line) vehicles for combined case in 71.89–52.05 km altitude region.

For some values of the relevant parameters, the resulting transform is extremely sensitive to not only the stability parameter and roll-rate altitude profiles, but also the initial conditions, the viewing conditions, and the choice of integration endpoints. This sensitivity appears to be similar to the sensitivity of Lissajous figures to phase differences. Although this sensitivity is desirable for detecting small changes in the various inputs, obtaining an adequate fit to prechange data may be difficult if small changes to the input parameters results in large variations in the expected spectrum. It is important to emphasize that the appearance of the various features which have been illustrated in this section may be masked for slightly different sets of initial or viewing conditions or choice of integration endpoints. In addition, side lobes may appear in individual frames which may mimic details of features which are not present. For example, in the nonrolling cases in Figs. 4 and 6, the side lobe adjacent to the main lobe makes the actual singlets resemble the doublets expected for the rolling cases.

The number of free parameters that must be obtained by fitting can be minimized by:

1) Positioning the sensors at sufficient ranges that changes in the viewing condition parameters due to viewing geometry variations with RV altitude may be neglected.

2) Parameterizing the altitude variations of the stability parameter and the roll rate so that only the relevant parameters and not the actual values at each altitude point are determined by the fitting procedure (data quality may not justify attempts to extract anything but an altitude-averaged stability parameter).

3) Noting that the high-altitude roll rate, a parameter in any likely parameterization of the roll-rate history, may be obtained from either the high-altitude modulation or from exoatmospheric radar data. (Emphasizing the second-order modulation by sensor positioning simplifies the determination of the high-altitude roll rate.)

The number of data sets may be maximized by dividing the initial sensor data into the largest possible number of segments consistent with adequate resolution. Using data from multiple sensors serves both to increase the number of data sets and to resolve ambiguities between the roll rate and stability parameter profiles and the viewing conditions.

V. Conclusions

In this paper, the expected spectra of the body-motion-induced modulation in radar and optical data from the early re-entry region in the frequency domain canonical to the square root of the air density at the RV altitude was examined. In this domain, transforms of lengths sufficient to resolve roll-related features can be performed without masking due to changes in the planar oscillation frequency. Modulation mechanisms that depend linearly and quadratically on vehicle angle of attack result in up to six frequency components in this space. For rolling RV's, the contributions from the linear terms were distinctly different from those of the quadratic terms. Particularly in the quadratic case, the signatures expected from rolling and nonrolling Rv's show distinct differ-

ences particularly at high altitudes and low roll rates. Altitude-dependent stability parameter and roll-rate altitude profiles can be obtained by inverting the model signatures by comparing field and theoretical spectra.

Acknowledgments

The author would like to thank Andy Anderson, Kenneth Beckman, David Lush, Jay Morgan, and John Morris for their helpful suggestions.

References

[1]Petty, C., Norling, R., and Brennan J., "Optical Scintillations From Re-entering ICBM Nose Cones," Avco Everett Research Lab, Avco Corp., Everett, MA, RN 231, May 1961, also: AFBMD-TN-61-28.

[2]Leon, H. I., "Angle-of-Attack Convergence of a Spinning Missile Descending Through the Atmosphere," *Journal of Aerospace Sciences,* Vol. 25, Aug. 1958, pp. 480–484.

[3]Platus, D. H., "Angle-of-Attack Convergence and Windward-Meridian Rotation Rate of Rolling Re-Entry Vehicles," *AIAA Journal,* Vol. 7, Dec. 1969, pp. 2324–2330.

[4]Tolosko, R. J., "Effects of Initial Body Motion on Transient Amplification," *AIAA Journal,* Vol. 8, June 1970, pp. 1168–1170.

[5]Tolosko, R. J., "Re-Entry Dynamics of a Trimmed Body with Constant Spin," *Journal of Spacecraft and Rockets,* Vol. 8, Jan. 1971, pp. 21–27.

[6]Platus, D. H., "Re-entry Vehicle Dispersion from Entry Angular Misalignment," *Journal of Guidance and Control,* Vol. 2, July-Aug. 1979, pp. 276–282.

[7]Nicolaides, J. D., "On the Free-Flight Motion of Missiles Having Slight Configurational Asymmetries," Ballistic Research Lab., Aberdeen, MD, Rept. 858, June 1953.

[8]Friedrich H. R. and Dore, F. J., "The Dynamic Motion of a Missile Descending Through the Atmosphere," *Journal of Aerospace Sciences,* Vol. 22, Sept. 1955, pp. 628–638.

[9]Allen, H. J., "Motion of a Ballistic Missile Angularly Misaligned with the Flight Path Upon Entering the Atmosphere and its Effect Upon Aerodynamic Heating, Aerodynamic Loads, and Miss Distance," NACA TN-4048, June 1956.

[10]Garber, T. B., "On the Rotation Motion of a Body Re-Entering the Atmosphere," *Journal of the Aerospace Sciences,* Vol. 26, July 1959, pp. 443–449.

[11]Norling, R. A., "Altitude of Stabilization for Slowly Tumbling Re-Entry Vehicles," *ARS Journal,* Vol. 32, Dec. 1962, pp. 1867–1870.

[12]Glover, L. S., "Effects on Roll Rate of Mass and Aerodynamic Asymmetries for Ballistic Re-Entry Bodies," *Journal of Spacecraft and Rockets,* Vol. 2, March–April 1965, p. 220–225.

[13]Waterfall, A. P., "Effect of Ablation on the Dynamics of Spinning Re-Entry Vehicles," *Journal of Spacecraft and Rockets,* Vol. 6, Sept. 1969, pp. 1038–1044.

[14]Murphy, C. H., "Angular Motion of Spinning Almost Symmetric Missiles," *Journal of Guidance and Control,* Vol. 2, Nov.–Dec. 1979, p. 504–510.

[15]Regan, F. J., *Re-Entry Vehicle Dynamics,* AIAA, New York, 1984, pp. 235–265.

[16]Platus, D. H., "Ballistic Re-Entry Vehicle Flight Dynamics," *Journal of Guidance and Control,* Vol. 5, Jan.–Feb. 1982, pp. 4–16.

[17]Berman R. J. and Storer, E. M., "Aerodynamic Drag Matrix," General Electric Working Paper No. 12, DIN: 6568-28-5, Feb. 1966.

[18]*U.S. Standard Atmosphere, 1962,* U.S. Government Printing Office, Washington, DC, Dec. 1962, pp. 36–59.